Silver and Caesium Diffusion Dynamics at the β-SiC Σ5 Grain Boundary Investigated with Density Functional Theory Molecular Dynamics and Metadynamics.

ARTICLE *in* THE JOURNAL OF PHYSICAL CHEMISTRY A · JANUARY 2014

Impact Factor: 2.69 · DOI: 10.1021/jp411156c · Source: PubMed

3 AUTHORS, INCLUDING:

Eddie López-Honorato
Center for Research and Advanced Studies of t…
36 PUBLICATIONS **276** CITATIONS
SEE PROFILE

P. Van Uffelen
Institute for Transuranium Elements
58 PUBLICATIONS **272** CITATIONS
SEE PROFILE

THE JOURNAL OF PHYSICAL CHEMISTRY A

Article

pubs.acs.org/JPCA

Silver and Cesium Diffusion Dynamics at the β-SiC Σ5 Grain Boundary Investigated with Density Functional Theory Molecular Dynamics and Metadynamics

Jeremy Rabone,*[,†] Eddie López-Honorato,[‡] and Paul Van Uffelen[†]

[†]European Commission, Joint Research Centre, Institute for Transuranium Elements, D-76125 Karlsruhe, Germany

[‡]Centro de Investigación y de Estudios Avanzados del IPN (CINVESTAV), Unidad Saltillo, Industria Metalúrgica 1062, Parque Industrial, Ramos Arizpe, 25900, Coahuila, México

Supporting Information

ABSTRACT: The diffusion and release of silver-110m, a strong γ-radiation emitter, through silicon carbide in coated nuclear fuel particles has remained an unsolved topic since it was first observed 40 years ago. The challenge remains to explain why, contrary to other elements, silver is capable of escaping the ceramic diffusion barriers. The current work investigates the underlying differences in the diffusion of silver and cesium along a symmetric tilt Σ5 grain boundary of β-SiC through accelerated density functional theory molecular dynamics simulations. The energy barriers extracted from the simulations give diffusion coefficients that are in reasonable agreement with experiment for silver (2.19×10^{-19} to 1.05×10^{-17} $m^2 s^{-1}$), but for cesium the equivalent calculated coefficients for this mechanism are much smaller (3.85×10^{-23} to 2.15×10^{-21} $m^2 s^{-1}$) than those found experimentally. Analysis of the simulated structures and electron densities and comparisons with the calculations of other researchers suggest that diffusion of silver and cesium in β-SiC proceeds via different mechanisms. The mechanisms of cesium diffusion appear to be dominated by its relatively large size and repulsive interactions with the silicon and carbon atoms; β-SiC grain boundaries still offer higher energy barriers to diffusion. Silver, on the other hand, is not only smaller in size but, as we show for the first time, can also participate in weak bonding interactions with the host atoms where favorable geometries allow, thus reducing the energy barrier and enhancing the rate of diffusion.

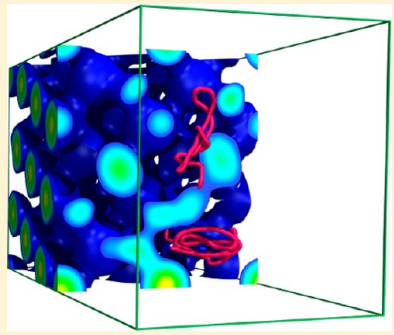

INTRODUCTION

The mobility of fission products within a nuclear reactor core presents challenges for containment, particularly under off-normal conditions, and is an important safety issue. The high-temperature reactor relies on the quality of its fuel, known as TRISO (tristructural isotropic) coated fuel particles, to maximize containment of fission products within the fuel itself. This fuel is made of a uranium kernel (300−500 μm in diameter) coated with three layers of pyrolytic carbon and one of silicon carbide (β-SiC), thus creating a miniature fission product containment vessel. The high structural strength of β-SiC and its chemical inertness, even at elevated temperatures, combined with the relative ease of coating fabrication make it an attractive material for this application.

Understanding the mechanisms by which fission products can cross the β-SiC barrier in TRISO particles is of great interest for their use in reactors. The diffusion of silver (particularly ^{110m}Ag which is a strong γ-emitter) has received particular attention owing to the apparently greater rate of diffusion across β-SiC coatings compared to other elements.[1−3] For over four decades scientists have tried to explain this phenomenon, and although different theories have been suggested to explain the diffusion of silver, for example, the presence of excess silicon or nanocracks,[3,4] recent integral release experiments of silver trapped between β-SiC layers suggest that grain boundary diffusion is the most likely mechanism for silver release from β-SiC coatings.[5] Bulk diffusion almost certainly makes a negligible contribution to transport in coatings on the basis of the energy barriers obtained from density functional theory (DFT) calculations and the lack of diffusion in single crystal experiments.[6,7] Furthermore, the results obtained by López-Honorato et al.[5] suggested that diffusion of silver is strongly related to the microstructure, or more specifically the characteristics of the grain boundaries involved. Because the microstructure depends on the deposition conditions used, samples made using methods other than fluidized bed chemical vapor deposition are likely to behave differently than β-SiC in fuel particles. Therefore, the value of the experiments carried out on β-SiC wafers generally used in the past, where no Ag diffusion was observed, is that β-SiC can be an effective barrier against the diffusion of silver if the microstructure is the right one.[4,6] Because the microstructure of these experiments was not

Received: September 11, 2013
Revised: January 13, 2014
Published: January 14, 2014

evaluated, little is known about what characteristics the β-SiC must have in order to be an effective barrier against diffusion.

In order to assess the effects of individual microstructures (e.g. grain boundaries) on diffusion within β-SiC, it is necessary to control which microstructures are present. However, silicon carbide produced by fluidized bed chemical vapor deposition is not obtained under constant conditions as the substrate moves up and down the bed of particles where concentration and temperature gradients exist. Therefore, it is not technically feasible to fabricate β-SiC coatings where only one variable in the microstructure is changed, such as the production of β-SiC with only one type of grain boundary. This difficulty can be overcome by computer modeling, where the degrees of freedom can be controlled.

The grain boundaries of β-SiC have previously been simulated using empirical potentials,[8] tight binding,[9] and ab initio[10] methods, to cite but a few of the many references, and can be well-modeled using these methods. The diffusion of silver and cesium in bulk β-SiC has also been investigated using static DFT calculations,[7,11] finding high energy barriers for the proposed mechanisms of bulk diffusion. Similar calculations applied to grain boundaries, e.g., ref 12, have identified lower energy barriers supporting a grain boundary diffusion process. The high temperature of reactor operation, and hence the thermal motion of both the diffusing species and the atoms of the grain boundary, make it desirable to carry out complementary studies of such systems dynamically. DFT calculations using optimized localized basis sets enable molecular dynamics (MD) simulations to be carried out using the forces obtained from DFT, allowing for the structural flexibility which is more difficult to incorporate in empirical potentials. The aim of this work is to provide a better understanding of the origin of the observed faster diffusion of silver compared to other elements such as cesium, which is commonly used as a reference element in experimental work. To this end we have applied density functional theory molecular dynamics to compare the high-temperature diffusion behavior of silver and cesium atoms at the relatively high-energy Σ5 (120) grain boundary of β-SiC.

It should be stressed that within the simulation size and time scales accessible using DFT, along with the inherent complexity of diffusion in a polycrystalline material such as β-SiC, one cannot expect to directly obtain a complete picture of the diffusion process. However, even simulations of diffusion along a single grain boundary can provide details of the electronic structure and offer instructive general insights into the interactions between grain boundaries in β-SiC and silver and cesium. As Ag diffusion has already been modeled in one type of Σ3 grain boundary using DFT, giving estimates of the diffusion coefficients,[12] it is also important to characterize other types of grain boundary structures to understand how various boundary environments could influence the diffusion behavior and diffusion rates. This is the motivation behind the selection of the relatively high-energy Σ5 boundary, which offers a significantly different set of atomic configurations compared to the Σ3 boundary and can exemplify how different grain boundary structures influence diffusion rates.

COMPUTATIONAL METHODS

There are several reasons for using a combination of static and dynamic DFT calculations for this study. A common issue encountered during static structure optimization is that the final structure can often be a local minimum. This is especially true when idealized starting structures are used in which the symmetry must be broken in order to access less symmetric but lower-energy structures. Dynamic calculations, as a consequence of random thermal motion, are able to escape local minima more easily. However, in dynamic structures it is more difficult to separate the thermal effects between different simulations; hence, it is often desirable to carry out static minimizations starting from the instantaneous coordinates of a simulation. An additional bonus of dynamic simulations for the study of diffusion, when suitably accelerated, is that they can probe diffusion events in an unbiased fashion, allowing for modes of diffusion which might not be obvious from static models.

The calculations were carried out using the QUICKSTEP[13,14] module of CP2K (development version 2.2.214)[15] with a mixed Gaussian and plane wave basis.[16] Periodic boundary conditions were applied in all three dimensions. The spin-polarized PBE functional was used[17] with Goedecker–Teter–Hutter (GTH) pseudopotentials[18−20] incorporating scalar-relativistic core corrections. The orbital transformation method[21] was employed for an efficient wave function optimization. In both carbon and silicon the outer 4 electrons ($2s^2 2p^2$ and $3s^2 3p^2$) were treated as the valence shell, whereas for cesium the outer 9 electrons ($5s^2 5p^6 6s^1$) and for silver the outer 11 electrons ($4d^{10} 5s^1$) were treated as valence electrons. Contracted Gaussian basis sets of DZVP quality were used with a grid cutoff of 200 hartree.[22] Although the basis sets had been optimized to reduce the basis set superposition contributions (BSSE) to the system energy, these have been taken into account when comparing energies. The counterpoise correction method of Boys and Bernardi was used,[23] in which the energies are adjusted to take into account the lowering of the energy caused by the overlap of basis functions between neighboring atoms. This correction is applied by correcting for the difference in energy between isolated atoms and the energy of these atoms when the basis sets of all the other atoms in a particular structure are included without the atoms themselves (referred to as "ghost" atoms). This gives a good approximation of the energy lowering that results solely from the overlap of basis sets between nearby atoms. The corrections were calculated for each nonequivalent atom in each of the different atomic environments because the BSSE can depend strongly on the disposition of the surrounding atoms.

For the comparative calculations using the plane wave code VASP,[24−28] full structure optimizations were carried out (using the flag ISIF = 3 for bulk phases, which relaxes the cell shape and volume in addition to the atom positions, or ISIF = 2 for molecules, which relaxes the atom positions without altering the cell shape) with no symmetry constraints (with the flag ISYM = 0, which suppresses the symmetrization of charge densities and forces). A plane wave cutoff of 600 eV was used with suitably dense Monkhost–Pack k-point sampling meshes for the bulk materials while atom and molecule calculations were carried out at the γ-point in a 20 Å cubic box. Gaussian smearing of the electron occupations was applied (selected using the flag ISMEAR = 0) with a broadening of 0.05 eV (the flag SIGMA = 0.05 was used to set the width of the smearing).

The molecular dynamics simulations were carried out in the Born–Oppenheimer approximation using a time step of 1 fs with the always stable predictor–corrector (ASPC) method[29] in a constant pressure and temperature ensemble, thus allowing full flexibility of the simulation cells. The canonical sampling through velocity rescaling (CSVR) thermostat–barostat[30] was

used with a time constant of 10 fs for equilibration and 1000 fs for simulations.

The antiphase Σ5 (120) tilt grain boundary was chosen as the initial model for this study because of its short period, allowing the use of a relatively small unit cell, as well as the apparent volume available for interstitial atoms at this boundary (Figure 1). The symmetry about the (120) plane makes this

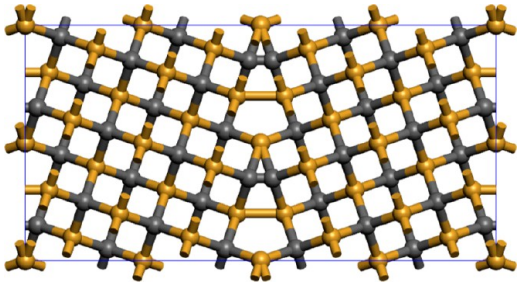

Figure 1. Initial unit cell of the (120) antiphase, tilt grain boundary (Σ = 5; tilt angle, 36.87°). Silicon atoms are depicted in yellow and carbon atoms in gray.

grain boundary convenient to model using periodic boundary conditions because the simple unit cell comprises two identical grain boundaries. Other grain boundaries, such as Σ3 (211) and Σ9 (221) that are more common in polycrystalline β-SiC at room temperature,[31,32] would require incorporation of two nonidentical grain boundaries in a simulation cell in order to maintain stoichiometry (see Supporting Information for details). Similar study for these type of grain boundaries is underway, and the results will be published elsewhere. The bicrystal approach, which has also been used to study grain boundaries in β-SiC, can be used to replace one of the boundaries with a vacuum gap, but energy of the surfaces so introduced cannot be calculated independently (the simple slabs would be terminated with two nonequivalent surfaces). It would also be less desirable to use this approach with DFT-MD simulations because to maintain the stability of the system the coordinates of atoms at the surface boundaries would require fixing, thereby affecting the atomic motion over relatively large distances and so necessitating the use of larger simulation cells.

This cell was first geometry optimized followed by a short MD equilibration at 1500 K. Two new simulation cells were defined using the coordinates obtained from the MD equilibration with silver and cesium atoms placed at the center of the cell. Further MD equilibrations and then simulations were run at 1500 K on these two cells to allow them to relax. The structures so obtained were used as the starting points for diffusion simulations.

As diffusion is a relatively slow process at the time scales accessible using atomistic modeling, which is especially true of DFT-based methods, it is necessary to accelerate the simulated dynamics. In this investigation we have used the metadynamics[33,34] methods available in CP2K to force the silver and cesium atoms out of their initial locations at the grain boundary. The collective variables used for the metadynamics were the distances along the Cartesian y and z directions between the silver and cesium atoms and the center defined as the average of all the silicon and carbon atoms located more than 1.9 Å from the plane of the grain boundary (Figure S1 of Supporting Information). Using the atoms away from the boundary removes much of noise which would otherwise arise from the motion of atoms at the grain boundary. During the metadynamics simulations, Gaussian potentials were placed every five steps (5 fs) of the simulation such that the silver and cesium atoms were stimulated to explore the grain boundary by the potential

$$V(t) = 0.01 \sum_{i=1}^{N(t)} \left(\exp\left[-\frac{1}{2}\left(\frac{y(i) - y(0)}{0.01} \right)^2 \right] \times \exp\left[-\frac{1}{2}\left(\frac{z(i) - z(0)}{0.01} \right)^2 \right] \right)$$

where $V(t)$ is the history-dependent potential, in hartrees, at time step t and $N(t)$ is the number of accumulated distance variables, y and z, in angstrom. During the metadynamics simulation, this potential gradually builds up until it is sufficient to force the silver or cesium atoms over an energy barrier. Unlike in nudged elastic band calculations, in which the start and end points of the trajectory are predetermined, the atoms in a metadynamics simulation are free to explore the available energy landscape of the system as it undergoes both the thermal vibrations and mutual interaction with the diffusing atoms. Providing the Gaussian potentials are not so strong or placed so often that they force the whole system into an unlikely high-energy configuration, this allows energy barriers to be sampled in an unbiased manner while incorporating the thermal motions of the atoms which may open or close lower-energy diffusion pathways over time. The system trajectories and energy profiles become more complicated to interpret, however, because the thermal motion causes significant perturbations of both energy and atomic positions. By careful averaging of the system energy and identification of the points at which events start and end, it is still possible to recover reasonable estimates of the energy barrier heights along with uncertainties resulting from the thermal motion. The energies of the sampled barriers can then be used to calculate diffusion coefficients by treating the diffusion as an activated random walk.

In principle it would also be possible to construct the complete free-energy landscape for the grain boundary diffusion using this approach. This was not attempted on this occasion because to obtain accurate energy surfaces a considerably more complete sampling of the configuration space would be needed, thus necessitating a greater number of longer simulations.

Validation of Simulation Parameters. Initial CP2K calculations were performed to determine the size of supercells required to obtain well-converged properties. Table 1 shows the convergence of properties with respect to supercell size for calculations of diamond, silicon, and β-SiC. The properties of β-SiC converge quickly with supercell repeats and the 3 × 3 × 3 supercell was considered to be sufficiently well-converged.

To assess the performance of the carbon and silicon pseudopotentials and DZVP basis sets employed in the CP2K calculations, the results obtained for some convenient C/Si reference structures are compared with experiment and equivalent calculations using VASP in Table 2. The cohesion energies calculated with CP2K are consistently lower than those calculated with VASP because the DZVP basis sets used in CP2K, while optimized for molecules and solids, give proportionately lower atomic energies and consequently increase the apparent cohesion energies. Better agreement between VASP and CP2K is therefore obtained by comparing

dx.doi.org/10.1021/jp411156c | J. Phys. Chem. A 2014, 118, 915−926

Table 1. Convergence of Bulk Properties with Respect to the Size of the Supercell for β-SiC, Diamond, and Silicon

supercell	1 × 1 × 1	2 × 2 × 2	3 × 3 × 3	4 × 4 × 4
E_{coh} (4 × SiC) (eV)	−45.37	−55.49	−55.96	−56.00
$a = b = c$ (Å)	4.452	4.372	4.370	4.370
$\alpha = \beta = \gamma$ (deg)	90.00	90.00	90.00	90.00
mean Si−C (Å)	1.928	1.893	1.892	1.892
E_{coh} (8 × C) (eV)	−56.51	−70.72	−71.36	−71.41
$a = b = c$ (Å)	3.703	3.582	3.575	3.575
$\alpha = \beta = \gamma$ (deg)	90.00	90.00	90.00	90.00
mean C−C (Å)	1.603	1.551	1.548	1.548
E_{coh} (8 × Si) (eV)	−26.81	−35.78	−36.51	−36.60
$a = b = c$ (Å)	5.620	5.473	5.459	5.457
$\alpha = \beta = \gamma$ (deg)	90.00	90.00	90.00	90.00
mean Si−Si (Å)	2.433	2.370	2.364	2.363

Table 2. Cohesion Energies Calculated Using CP2K (Corrected for BSSE) and VASP Compared with Experiment

	E_{coh} (eV)			BSSE (eV)	
structure	CP2K	VASP	expt	C	Si
diamond (8 × C)	−60.55	−62.80	−59.30	−1.36	–
silicon (8 × Si)	−36.24	−36.95	−37.81	–	−0.05
Si_2C_2(g)	−17.34	−18.23	−17.29	−1.29	−0.01
β-SiC (4 × SiC)	−50.24	−52.04	−51.66	−1.40	−0.04
α-SiC (6 × SiC)	−75.18	−78.06	−77.43	−1.41	−0.05

energies for reactions between solid phases and the Si_2C_2 molecule.

For diamond, silicon, and β-SiC, 4 × 4 × 4 supercells were used for the CP2K calculations while the VASP calculations used single unit cells and a 6 × 6 × 6 MP k-point sampling grid. For the hexagonal α-SiC, a 5 × 5 × 1 supercell was used in CP2K and a 7 × 7 × 3 MP k-point sampling grid used in VASP. For the Si_2C_2 molecule, the singlet rhombus configuration previously identified as the lowest-energy structure was used.[35]

The calculated energies for reactions between the different compounds are in reasonable agreement (excluding dispersion, thermal, and zero-point contributions to the calculated energies):

$$C(s) + Si(s) \rightarrow \beta\text{-}SiC(s)\ \ \Delta H_{CP2K} = -0.46\text{eV},$$
$$\Delta H_{VASP} = -0.54\text{eV},\ \Delta H^{\ominus}_{exp} = -0.78\text{eV}$$

$$\frac{1}{2}Si_2C_2(g) \rightarrow \beta\text{-}SiC(s)\ \ \Delta H_{CP2K} = -3.89\text{eV},$$
$$\Delta H_{VASP} = -3.90\text{eV},\ \Delta H^{\ominus}_{exp} = -4.27\text{eV}$$

$$\alpha\text{-}SiC(s) \rightarrow \beta\text{-}SiC(s)\ \ \Delta H_{CP2K} = -0.03\text{eV},$$
$$\Delta H_{VASP} = -3 \times 10^{-4}\text{eV},\ \Delta H^{\ominus}_{exp} = -0.01\text{eV}$$

A plot of the calculated phonon density of states for bulk β-SiC is compared with plane wave calculation and experimental data in Section S1 of the Supporting Information. Reference calculations for silver and cesium compounds are given in Section S2 of the Supporting Information.

The calculated formation energies of neutral, singlet carbon, and silicon vacancies and interstitials and substitutions in β-SiC are summarized in Table 3. The defect formation energy has been defined as

Table 3. Calculated Defect Formation Energies in β-SiC for the Neutral, Singlet States and Corrected for BSSE[a]

	defect formation energy (eV)	
	wrt free atom	wrt β-SiC (±0.28 eV)
C vacancy	12.20	4.41
Si vacancy	11.94	7.19
C interstitial C void	−0.54	7.25
C interstitial Si void	−0.54	7.25
Si interstitial C void	3.83	8.58
Si interstitial Si void	5.70	10.45
C substituting Si	0.40	3.44
Si substituting C	5.49	2.45

[a]The values in the left column are taken relative to the free C or Si atom and thus include relatively large contributions from the high energies of isolated atoms. The values in the right column are taken relative to calculated chemical potentials for C or Si atoms in β-SiC (taken as the calculated cohesion energies of bulk diamond and silicon plus half the formation energy of β-SiC, giving −7.79 and −4.75 eV, respectively) and thus give a better indication of the relative likelihood of defect formation. The ±0.28 eV in energy represents the maximum permissible variation in these energies in the absence of precise values for the calculated chemical potential.

$$\Delta E = E(\text{defect cell}) - E(\beta\text{-SiC}) - N_C \times E(C) - N_{Si} \times E(Si)$$

where E are the calculated energies for the defect cell, bulk β-SiC, a carbon atom, and a silicon atom and N_C and N_{Si} are the numbers of extra carbon and silicon atoms in the defect structure (a negative number is used where the defect contains fewer atoms).

The starting structures for the interstitials were with the extra atom at a tetrahedral void with either four carbon atoms (C void) or four silicon atom (Si void) closest to the interstitial. These values are consistent with the results from previous DFT calculations, e.g., see ref 7, although there are many more possible configurations for interstitials than presented here. In all except the C interstitials the defect retains the initial tetrahedral symmetry around the defect; both of the carbon interstitials relax to give a structure with the carbon atom bonded to two other carbon atoms and a Si atom.

RESULTS AND DISCUSSION

Structure and Energy of the Grain Boundary. The (120) grain boundary structure is maintained during structure optimization (Figure 2), undergoing slight expansion perpen-

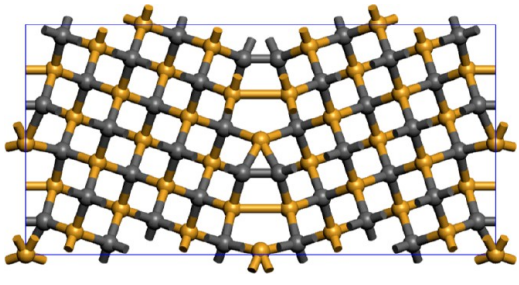

Figure 2. Cell obtained after structure optimization of the (120) grain boundary. Silicon atoms are depicted in yellow and carbon atoms in gray.

dx.doi.org/10.1021/jp411156c | J. Phys. Chem. A 2014, 118, 915−926

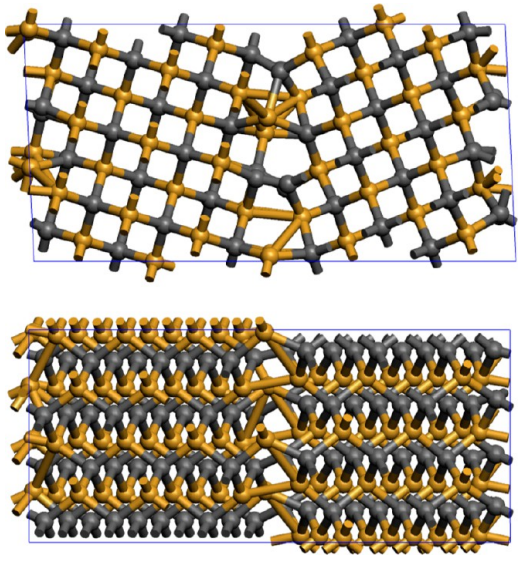

Figure 3. Top and front views of the distorted cell obtained after static optimization of the structure obtained following 1 ps of MD equilibration. Silicon atoms are depicted in yellow and carbon atoms in gray.

dicular to the boundary which relieves the strain of the close C−C contacts. The surface formation energy relative to the bulk is given by

$$\Delta E = \frac{E(\text{grain boundary}) - E(\beta\text{-SiC})}{\text{area}}$$

where E are the calculated energies of the grain boundary structure and bulk β-SiC with the same number of atoms (allowing for changes in the BSSE of atoms at the boundary, which were found to be practically negligible) and area is the total area of the grain boundaries (i.e., twice the cross-sectional area of the cell because there are two boundaries). The surface formation energy relative to the bulk was calculated to be 3.80 J m^{-2}. A value of 3.75 J m^{-2} was obtained from structure optimization using the plane wave code VASP. For comparison, the results of calculations using several other grain boundaries are given in Section S3 of the Supporting Information.

During 1 ps MD equilibration at 1500 K, the structure underwent a symmetrical distortion in which the two sides of the grain boundary slid parallel to the grain boundary by about 0.35 Å and the cell angle changed by 2° (Figure 3). After structure optimization, the surface formation energy was calculated to be 3.35 J m^{-2}, indicating that the structure obtained from the direct structure optimization (Figure 2) is actually a local minimum. This was confirmed by a second VASP calculation which gave a value of 3.36 J m^{-2}.

During molecular dynamics simulations at 1500 K this structure is maintained, albeit with a larger motion (the average volume of the thermal ellipsoids for atoms near the grain boundary is 2.75 times that of the atoms in the bulk, and the frequency of the first peak in the vibrational power spectrum for the boundary atoms is about 60% that of the bulk atoms) in the atoms adjacent to the grain boundary (Figure 4). The

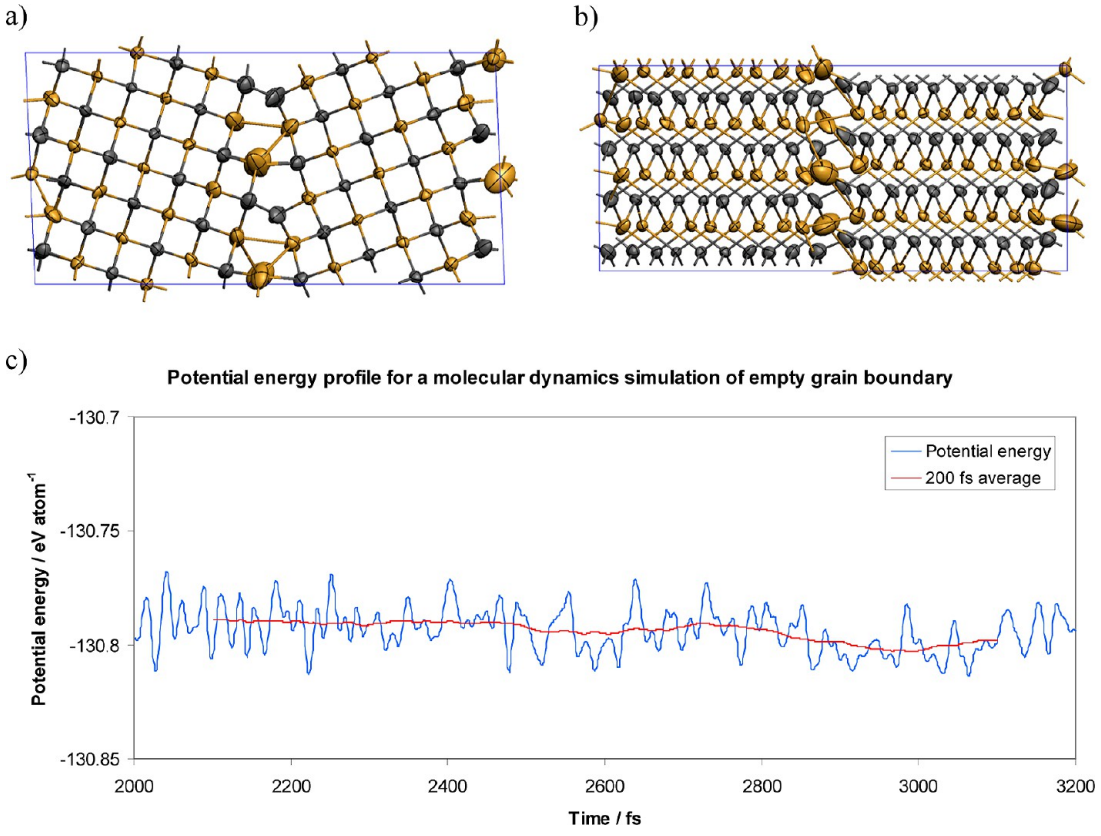

Figure 4. (a) Top and (b) front views of the distorted cell from a 1.2 ps MD simulation at 1500 K showing "thermal ellipsoids" at the 90% level of probability. (c) Potential energy profile of this simulation and the 200 fs average for comparison with results of metadynamics simulations that will be discussed later. Silicon atoms are depicted in yellow and carbon atoms in gray.

dx.doi.org/10.1021/jp411156c | J. Phys. Chem. A 2014, 118, 915−926

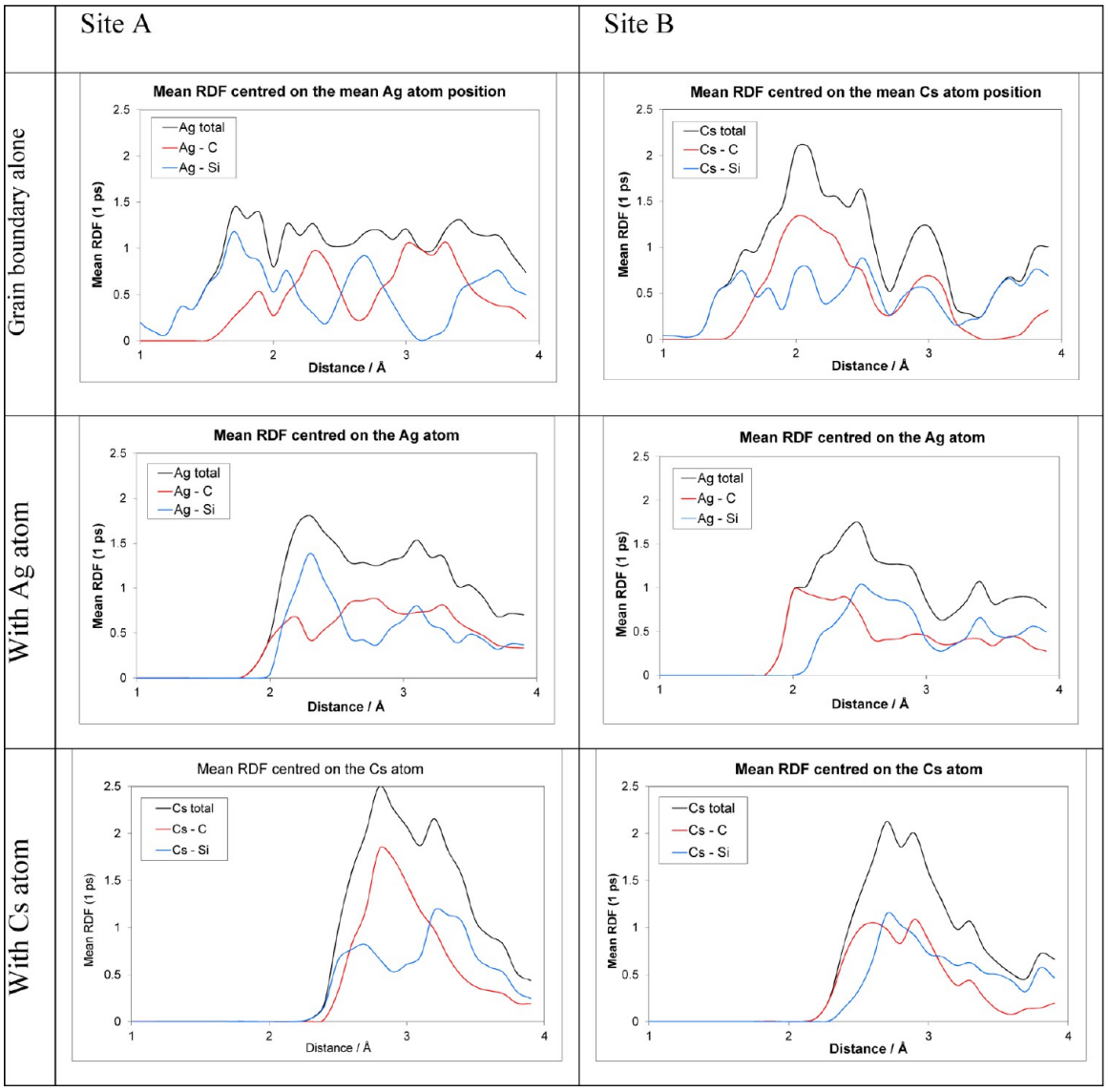

Figure 5. Time-averaged radial distributions functions (RDFs) calculated from 1 ps MD trajectories. Black, total; red, carbon; blue, silicon. The mean coordinates of the Ag and Cs atoms were used to define the centers of site A and site B for the RDFs from simulations of the grain boundary.

relative freedom of these atoms, mediated by the interaction with guest atoms, is a contributing factor to diffusion along the grain boundary.

Incorporation of Silver and Cesium in the Bulk and at the Grain Boundary. The calculations for Ag and Cs incorporated in bulk SiC were carried out on a 3 × 3 × 3 supercell at interstitial and in neutral vacancy sites. Two interstitial sites were investigated, one at the center of a tetrahedra of carbon atoms (interstitial-C) and the other at the center of a tetrahedral of silicon atoms (interstitial-Si). These defects retained tetrahedral symmetry during structure optimization except in the case of Cs in the interstitial-C. In this last case, the Cs atom moves to a new location, displacing a C and a Si atom along the ⟨111⟩ direction and coming to lie between them.

Despite starting from equivalent coordinates, the cells with the Ag and Cs atoms placed at the center relaxed to different configurations during the MD equilibration and simulation. The silver atom moved to an adjacent void of the grain boundary (site A, Figure 6a) while the cesium atom rebounded into the void it started in (site B, Figure 6b). Radial distribution functions (RDF) calculated from the MD simulation of the empty grain boundary (Figure 5) and the associated coordination numbers (Figure S6 of the Supporting Information) show the two sites possess subtly different environments even in the absence of guest atoms. Site A is slightly more crowded by silicon atoms at short-range (∼1.7 Å), whereas site B has a greater crowding by carbon atoms (∼2.0 Å). The reorganization of the grain boundary induced by the Ag and Cs atoms is driven by contacts with the silicon atoms, owing to both their larger size and greater prominence at the boundary (Figure 5). The larger size of the Cs atom results in the formation of RDFs that are more sharply peaked than those of the smaller Ag atom. The effective radius of the Cs atom from the RDFs is about 0.4 Å larger than that of the Ag atom (approximate literature values for the metallic, covalent, and ionic radii for Ag are 1.4 , 1.5, and 1.3 Å, respectively, while for Cs they are 2.7, 2.3, and 1.8 Å, respectively; for comparison, the covalent radius of C is 0.8 Å and that of Si is 1.1 Å). This combined with the greater prevalence of silicon atoms around

dx.doi.org/10.1021/jp411156c | J. Phys. Chem. A 2014, 118, 915−926

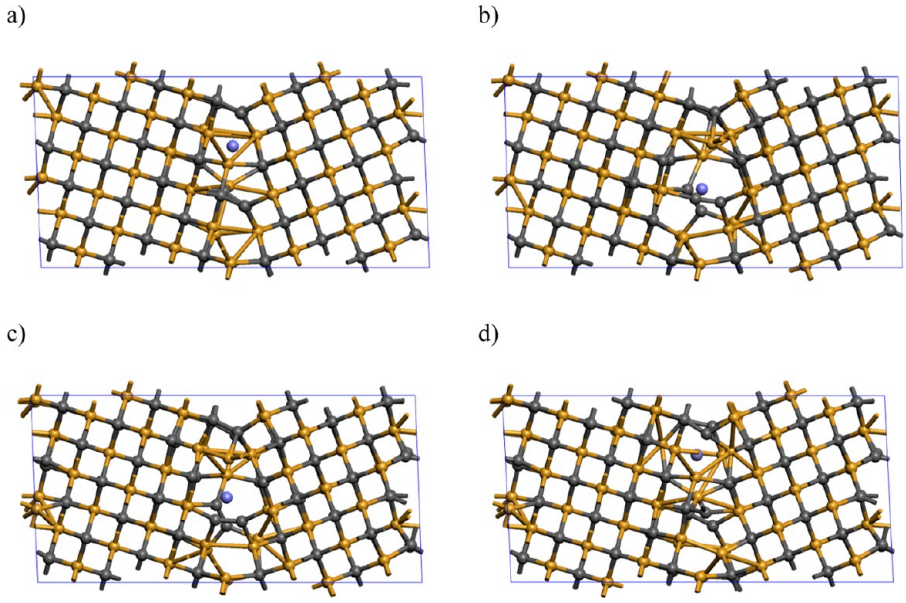

Figure 6. Structures obtained following MD simulation and static structure optimization of the grain boundary with (a) Ag at site A and (b) Cs at site B. The optimized structures when the Ag and Cs atoms are swapped are shown in (c) with Ag at site B and (d) with Cs at site A. The locations of the Ag and Cs atoms are show with a blue sphere; silicon atoms are depicted in yellow and carbon atoms in gray.

Table 4. Incorporation Energies for Ag, Cs, C, and Si in Bulk SiC, Neutral Vacancies, and at the Grain Boundary[a]

	incorporation energy (eV)			
	Ag	Cs	C	Si
interstitial-C	7.80	17.61	−0.54	3.83
interstitial-Si	8.78	24.44	−0.54	5.70
C vacancy	−1.04	6.56	−12.20	−6.72
Si vacancy	−3.30	4.65	−11.54	−11.94
GB site A	0.88	7.64	−8.90	−3.09
GB site B	1.19	8.87	−4.55	−2.35
GB site A − dynamic V	0.61	7.84	–	–
GB site B − dynamic V	1.12	8.69	–	–
GB site A − dynamic V+K	0.80	8.03	–	–
GB site B − dynamic V+K	1.32	8.88	–	–

[a]The incorporation energies are calculated relative to the energies of the bulk, vacancy, grain boundary, and the isolated atoms; the BSSE of the Ag, Cs, and Si atoms were negligible; these values have been corrected for the BSSE of C.

Table 5. Energies (in Electronvolts) Associated with the Exchange of Atoms between Incorporation Sites at a C or Si Bulk Vacancy and Grain Boundary Site A or Site B[a]

		C vacancy			Si vacancy		
		Si	Ag	Cs	Si	Ag	Cs
Site A	C	0.33	−1.38	−2.23	6.21	1.54	−1.05
	Si		−1.71	−2.56		−4.76	−5.86
	Ag			−0.85			−1.19
Site B	C	−3.29	−5.43	−5.35	2.59	−2.51	−4.18
	Si		−2.14	−2.06		−5.10	−5.37
	Ag			0.07			−0.27

[a]The exchange energy gives the relative stability of two configurations. For example the exchange of an Ag atom incorporated into a C vacancy site with a Si atom incorporated at grain boundary site A is associated with a lowering of energy (−1.71 eV).

site A is responsible for a remarkable difference in the resulting RDFs. For silver, a distinct peak is formed in the silicon RDF at 2.4 Å with some carbon atoms lying closer than the nearest silicon atoms. In the case of cesium, it is the silicon atoms that lie slightly closer and carbon atoms form a large peak at 2.9 Å. The explanation for this feature is that the displacement of the silicon atoms by the cesium atom at site A results in the carbon atoms bonded to the silicon being pulled taut, away from the cesium atom, forming a cage around it. The average coordination numbers within spheres of 2.5 Å radius around Ag and 2.9 Å radius around Cs are 2.5 (Ag−Si, Site A), 1.6 (Ag−C, Site A), 1.2 (Ag−Si, Site B), 2.7 (Ag−C, Site B), 2.5 (Cs−Si, Site A), 3.6 (Cs−C, Site A), 2.7 (Cs−Si, Site B), and 3.7 (Cs−C, Site B).

The final coordinates from these simulations were structure-optimized using the final coordinates from both simulations. A second MD equilibration and simulation followed by structure optimization was carried out starting from these structures with the Ag and Cs atoms switched between sites. The structures obtained after optimization are shown in Figure 6. These structures demonstrate the greater structural interference caused by the larger cesium atom in comparison to the silver atom. The grain boundary retains roughly the same structure in the presence of the silver atom (Figure 6a) while the cesium atom forces several of the boundary atoms to move to new locations (Figure 6b). The structural changes induced by the Cs atom during the dynamic simulation are only partially undone when the Cs atom is replaced by the Ag atom (Figure 6c). Conversely, substitution of the Ag atom by a Cs atom pushes several atoms away from the grain boundary (Figure 6d).

Table 4 gives incorporation energies for Ag, Cs, C, and Si in bulk β-SiC, in netural vacancies, and the grain boundary calculated according to

$$\Delta E = E(\text{cell incorporating atom}) - E(\text{cell without atom}) - E(\text{atom})$$

where E(cell incorporating atom) is the energy of the cell with the extra Ag, Cs, C, or Si atom; E(cell without atom) is the

dx.doi.org/10.1021/jp411156c | J. Phys. Chem. A 2014, 118, 915−926

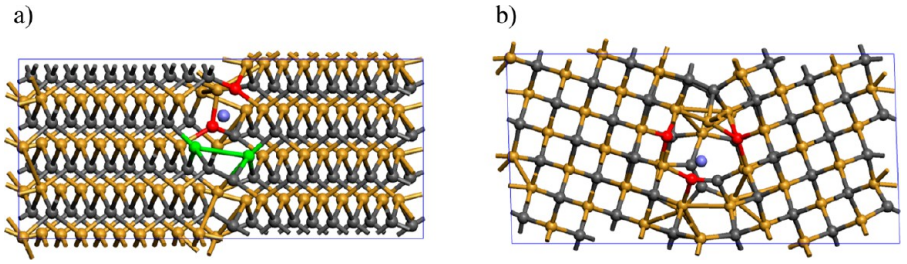

Figure 7. Structures obtained following MD simulation and static structure optimization of the grain boundary with (a) Ag at site A shown from the front and (b) Ag at site B shown from the top. The locations of the Ag atom are shown with a blue sphere. Triangularly coordinated carbon and silicon atoms which form a roughly tetrahedral arrangement around the silver atom are shown in red and green, respectively; other silicon atoms are depicted in yellow and carbon atoms in gray.

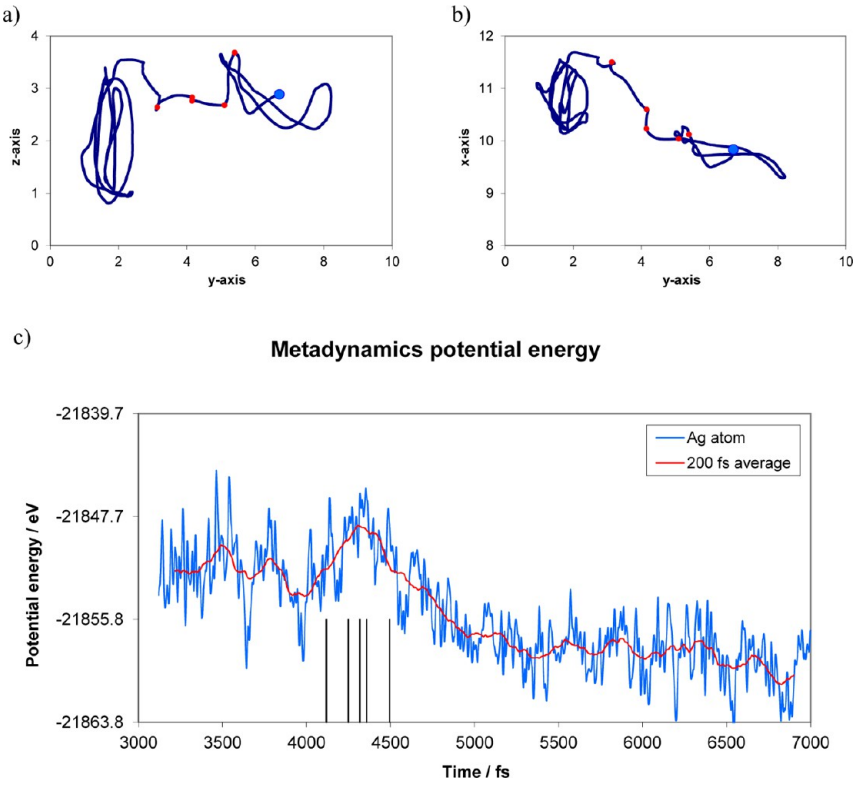

Figure 8. The trajectory and potential energy curve of the silver atom during the metadynamics simulation. Panels (a) and (b) show the $y-z$ and $x-y$ coordinates of the Ag atom; the blue dot indicates the start location of the atom, and the red dots indicate the start, midpoints, and end of the barrier crossing. These five points in time are indicated with vertical, black lines on the potential energy curve (c).

energy of bulk β-SiC for interstitials, the energy of the vacancy structure for the vacancy substitutions, or the energy of the grain boundary; and E(atom) is the energy of the isolated Ag, Cs, C, or Si atom. The dynamic incorporation energies were calculated from the averaged molecular dynamics potential energies (dynamic V) and total energies (dynamic V+K). The potential energies from the dynamics have been corrected for small variations in the simulation temperatures, which were 1452, 1495, 1517, 1465, and 1460 K for the GB, GB+Ag (site A), GB+Cs (site B), GB+Ag (site B), and GB+Cs (site A) structures, respectively. The incorporation energies in this table are taken as the difference in energy between the simulations with the Ag or Cs atom at the boundary and the simulation of the grain boundary alone and the isolated Ag or Cs atoms. As these energies are in relation to the isolated Ag or Cs atoms, they provide only a partial indication of the relative importance of these modes of incorporation. Building a full model of the thermodynamic distribution of Ag and Cs in SiC would require the chemical potentials of all of the possible modes of incorporation. However, the values in the table can be combined for some atom exchanges so that chemical potentials cancel; for example, Table 5 summarizes the energies of atom exchange between bulk vacancies and grain boundary sites.

From the energies given in Table 4 it is obvious that the silver atom is more easily accommodated in SiC than the cesium atom both at the grain boundary and in the bulk. Incorporation at site B is found to be higher in energy by about 0.9 eV for Cs and 0.5 eV for Ag compared to site A. The exchange energies in Table 5 suggest that there is strong preference for Ag and Cs to concentrate at the grain boundaries; Cs is slightly more preferential than Ag. Comparison of the energies of the statically optimized structures with those of the separated grain boundary and Ag or Cs components (Table S4 of the Supporting Information) shows that at both site A and site B not only does the Ag atom raise the energy of the grain boundary ~2 eV less than the Cs

dx.doi.org/10.1021/jp411156c | J. Phys. Chem. A 2014, 118, 915−926

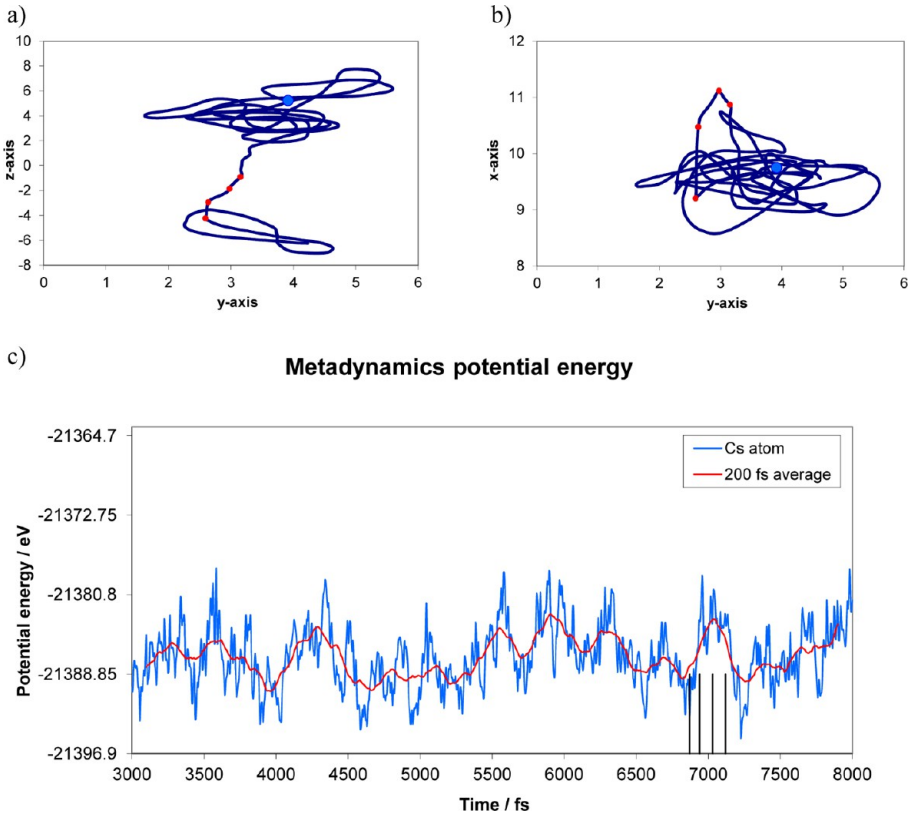

Figure 9. Trajectory and potential energy curve of the cesium atom during the metadynamics simulation. Panels (a) and (b) show the $y-z$ and $x-y$ coordinates of the Cs atom; the blue dot indicates the start location of the atom, and the red dots indicate the start, midpoints, and end of the barrier crossing. These four points in time are indicated with vertical, black lines on the potential energy curve (c).

atom but also the Ag atom has favorable interactions ($\Delta E \sim -2.3$ eV) with the distorted boundaries, whereas the Cs atom interacts unfavorably with the distorted boundaries ($\Delta E \sim +2.8$ eV). Mulliken population analyses from the calculations show significant electronic occupation of the 5s and 5p orbitals of Ag, indicating that the favorable interactions arise from the overlap of these orbitals of the Ag atom with partially occupied s- and p-orbitals of carbon and silicon atoms at the grain boundary. Geometries maximizing such interactions include those where the silver atom lies near one or more triangularly coordinated carbon or silicon atoms in roughly tetrahedral configurations, and these configurations can be observed in the calculations (Figure 7).

Bader analysis[36−38] of the charge densities from the statically optimized structures gives the Cs atom a Bader charge of +0.55 at the first site and +0.59 when at the swapped site. The Ag atom on the other hand has a Bader charge of −1.19 at the first site and −0.43 when swapped, thus suggesting stronger interactions with the atoms of the grain boundary. The unusually negative charge on Ag arises from the above-noted overlap of atomic orbitals of silver with adjacent atoms rather than formation of a silver anion. The presence of strong interactions in the case of Ag is further reinforced by charge density difference plots (Figure S5 of the Supporting Information), which show that the main differences are more localized around the silver atom than in the case of the cesium atom where they are more delocalized onto the atoms of the grain boundary.

Migration of Ag and Cs. Figures 8 and 9 show the results of the metadynamics simulations of the grain boundary with the silver and cesium atoms included. In each case the barrier crossing occurs when the Ag or Cs atom leaves the initial region and traverses into another part of the grain boundary. Kinks in the trajectories (shown with red dots in the figures) can be used to identify the start, end, and midpoints of the transitions. For the transition of the Ag atom, there are five distinct points on the trajectory, and for the transition of the Cs atom, there are four distinct points. An estimate of the barrier energy can be obtained from the difference in the 200 fs mean of the system potential energy at the start point and the energy maximum. The standard deviation of the mean can be used to give upper and lower bounds for this energy. On this basis the estimated barrier heights are 3.35 ± 0.250 eV in the case of the Ag atom and 4.65 ± 0.260 eV for the Cs atom. When the diffusion is treated as an activated random walk (details in Section S6 of the Supporting Information), the estimated diffusion coefficients based on these trajectories are in the range of 3.85×10^{-23} to 2.15×10^{-21} $m^2\ s^{-1}$(median, 2.88×10^{-22} $m^2\ s^{-1}$) for Cs and 2.19×10^{-19} to 1.05×10^{-17} $m^2\ s^{-1}$ (median, 1.51×10^{-18} $m^2\ s^{-1}$) for Ag at 1500 K. It is noted that the price for the accelerated dynamics is a roughly 2-fold increase in the uncertainty of the energy; the maximum standard deviation of the mean potential energy from the MD simulation of the empty grain boundary (Figure 4c) is equal to 0.116 eV.

The estimate of the diffusion coefficient for silver in a Σ5 (120) grain boundary is considerably higher than that obtained for the Σ3 (211) grain boundary (3.7×10^{-18} $m^2\ s^{-1}$ at 1873 K) using DFT and MD[12] and falls just below the range of values measured in fuel studies and ion implantation experiments ($1.6–7.0 \times 10^{-17}$ $m^2\ s^{-1}$ near 1500 K),[1,5] reinforcing the hypothesis that the presence of higher-angle grain boundaries

dx.doi.org/10.1021/jp411156c | J. Phys. Chem. A 2014, 118, 915−926

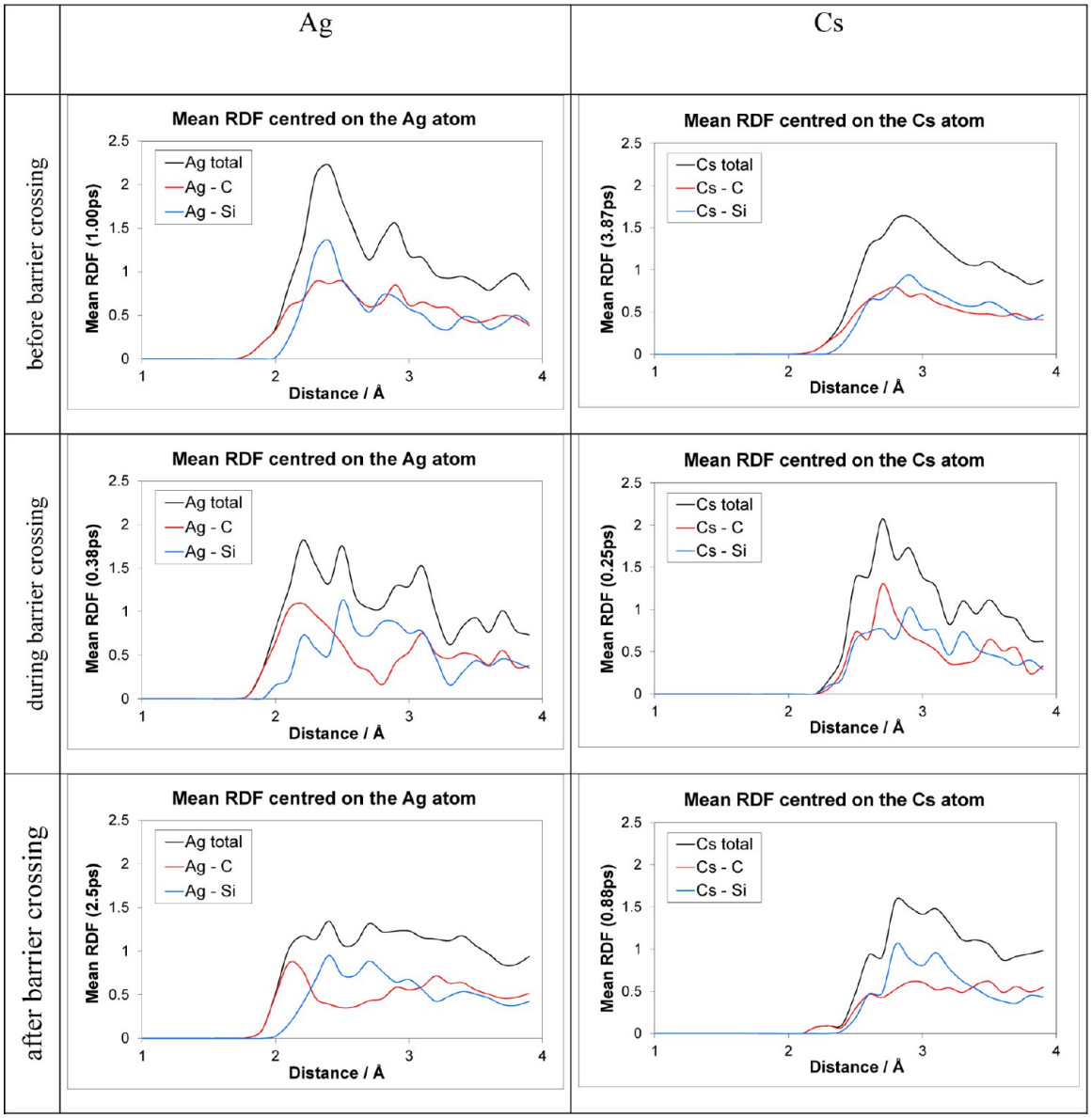

Figure 10. Time-averaged radial distributions functions calculated from the accelerated MD trajectories. Black, total; red, carbon; blue, silicon. The top row shows the period before the Ag and Cs atoms cross the energy barrier, the middle row during the transition, and the bottom row after the transition.

can considerably increase the diffusion of silver and are an important diffusion pathway. The higher diffusion rates from experiments suggest that other grain boundaries and junctions may offer even faster diffusion paths; porosity, if present, could also be a contributing factor in reactor fuel. The estimated diffusion coefficient for cesium is rather smaller than that reported experimentally (2.1×10^{-17} to 2.4×10^{-18} m^2 s^{-1} near 1500 K).[39−41] However, the energy barrier obtained is of a magnitude similar to that calculated using DFT for bulk diffusion of Cs (5.1 eV),[11] whereas the equivalent barrier for bulk Ag diffusion is much higher (7.9 eV).[7] This suggests that bulk diffusion and other possible mechanisms are of a prevalence similar to grain boundary diffusion for Cs. Recent DFT calculations[42] have also found that the energy of Cs−O coincorporation is lower than that of the incorporation of cesium alone, but the opposite is found for silver.

The atomic trajectories in the time regions of the boundary crossings show a clear difference between the way Ag and Cs move along the grain boundary. The Ag atom interacts more with the boundary atoms and apparently receives several "nudges" in the direction of motion during the transition giving a relatively broader profile (377 fs elapses between the start and end points) in the potential energy curve (Figure 8c). The Cs atom remains more distant from the boundary atoms and interacts less with them, completing the transition in a more rapid movement evidenced by the narrower barrier profile (250 fs elapses between the start and end points) in the potential energy curve (Figure 9c).

The electron density differences taken at the instant that Ag and Cs atoms cross the energy barriers (Figure S7 of the Supporting Information) and energy components (Table S5 of the Supporting Information) suggest that the positive interactions of Ag with the grain boundary atoms are reduced during the transition while the distortion energy of the boundary remains fairly constant. Conversely, the negative interactions between the Cs atom and the grain boundary

dx.doi.org/10.1021/jp411156c | J. Phys. Chem. A 2014, 118, 915−926

remain quite similar while the energy is increased significantly by the distortion of the grain boundary. These observations are consistent with interactions between the vacant 5p orbitals of Ag and the s and p orbitals of C and Si atoms lowering the energy when the local geometry is conducive to allow good overlap. These favorable interactions are subsequently reduced when the Ag atom moves to regions where geometrical constraints reduce the orbital overlap. For Cs it is the size of the atom and the distortion it induces in the grain boundary that creates the energy barrier.

Time-averaged RDFs around the Cs and Ag atoms over the metadynamics simulations before, during, and after the barrier crossings are shown in Figure 10 for comparison with the RDFs calculated from the unaccelerated molecular dynamics simulations (Figure 5). The RDFs indicate that silicon atoms are responsible for the constriction of the diffusion barriers. For both silver and cesium, during the barrier crossing a small shift to shorter range is observed in the RDFs for silicon while a small shift to longer range is found for the carbon RDFs.

Also shown in Figure S8 of the Supporting Information are time evolutions of coordination number (at ranges of 2.5 Å for Ag and 2.9 Å for Cs) during the simulations along with plots of coordination number against system energy. A weak correlation is observed between the coordination number and system energy for the Ag atom, which can be related to small reductions in both coordination number and energy after the barrier crossing. For Cs, there is no observable correlation between the coordination number and system energy. A weak correlation also exists between the system energy and how close the geometry around the Ag atom is to a tetrahedron (Figure S9 of the Supporting Information) while there is no such correlation for the Cs atom. This is further evidence of energy-lowering electronic interactions between the silver atom and the grain boundary.

CONCLUSIONS

The results of the accelerated DFT-MD simulations suggest that diffusion along high-angle grain boundaries of silicon carbide, such as the Σ5 symmetric tilt boundary, could play a role in the transport of silver from the fuel kernels of TRISO particles. The calculated energy barrier to the diffusion of silver in this grain boundary yields estimates for the diffusion coefficient that are reasonably close to experimentally observed ranges. Grain boundary diffusion is found to be less likely in the case of cesium; the calculated energy barrier leads to a diffusion coefficient that is orders of magnitude smaller than that found experimentally.

The underlying causes for the difference in diffusion rate between Ag and Cs are twofold. The larger size of the Cs atom in relation to the Ag atom is the most important factor causing a large distortion of the atoms around the Cs atom and so forming a cage which consequently impedes diffusion. The interactions between the Ag or Cs atoms and the distorted grain boundary are also an important factor, as these further increase the energy of the Cs−GB system by about 2.7 eV while for the Ag−GB system they reduce the energy by about 2.1 eV. The charge distributions around the Ag and Cs atoms indicate that Ag participates in weak bonding with the grain boundary atoms while the Cs does not. The bonding interactions of Ag are reduced when the atom moves along the grain boundary into regions where the local geometry reduces the favorable overlap of the Ag 5p orbitals with the Si and C s- and p-orbitals. In general, bonding interactions have the potential to increase or decrease diffusion rates by reducing the energies during barrier crossing or reducing the energies within the incorporation sites, respectively. Where the diffusion rate-limiting process involves atoms passing "bottlenecks" in the host structure, as is the case for the Σ5 grain boundary, the presence of weak bonding interactions aids diffusion by reducing the effective size of the atom in the bottleneck. At the less restrictive incorporation sites the effects of weak bonding interactions exert less influence on diffusion because the atom is still relatively free to move.

The results of the accelerated DFT-MD simulations show promise in the elucidation of the underlying mechanisms of fission product migration in silicon carbide coatings at a relatively modest computational cost: 1 ps of simulation can be turned around in about one core year. In future calculations we will investigate other important fission products in various grain boundaries, junctions, and defect structures of β-SiC to produce a more complete picture of these processes.

ASSOCIATED CONTENT

Supporting Information

Calculated phonon density of states for bulk β-SiC (Section S1), reference calculations for various silver and cesium compounds (Section S2), grain boundaries in β-SiC (Section S3), detailed analysis of structures from the unaccelerated MD simulations (Section S4), detailed analysis of structures from the accelerated MD simulations (Section S5), and calculation of the diffusion coefficients from accelerated dynamics (Section S6). This material is available free of charge via the Internet at http://pubs.acs.org.

AUTHOR INFORMATION

Corresponding Author

*Tel: +49 7247 951297. E-mail: jeremy.rabone@ec.europa.eu.

Notes

The authors declare no competing financial interest.

ACKNOWLEDGMENTS

This work was supported by the High Performance Computing facility of the Joint Research Centre, Ispra.

REFERENCES

(1) Van der Merwe, J. J. Evaluation of Silver Transport through SiC During the German HTR Fuel Program. *J. Nucl. Mater.* **2009**, *395*, 99−111.

(2) Minato, K.; Sawa, K.; Koya, T.; Tomita, T.; Ishikawa, A.; Baldwin, C.; Gabbard, W. A.; Malone, C. M. Fission Product Release Behavior of Individual Coated Fuel Particles for High-Temperature Gas-Cooled Reactors. *Nucl. Technol.* **2000**, *131*, 36−47.

(3) Nabielek, H.; Brown, P. E.; Offermann, P. Silver Release from Coated Particle Fuel. *Nucl. Technol.* **1977**, *35*, 483−93.

(4) MacLean, H. J.; Ballinger, R. G.; Kolaya, L. E.; Simonson, S. A.; Lewis, N.; Hanson, M. E. The Effect of Annealing at 1500°C on Migration and Release of Ion Implanted Silver in CVD Silicon Carbide. *J. Nucl. Mater.* **2006**, *357*, 31−47.

(5) López-Honorato, E.; Zhang, H.; DaXiang, Y.; Xiao, P. Silver Diffusion in Silicon Carbide Coatings. *J. Am. Ceram. Soc.* **2011**, *94* (9), 3064−3071.

(6) Friedland, E.; Malherbe, J. B.; Van der Berg, N. G.; Hlatshwayo, T.; Botha, A. J.; Wendler, E.; Wesch, W. Study of Silver Diffusion in Silicon Carbide. *J. Nucl. Mater.* **2009**, *389*, 326−31.

(7) Shrader, D.; Khalil, S. M.; Gerczak, T.; Allen, T.; Heim, A. J.; Szlufarska, I.; Morgan, D. Ag Diffusion in Cubic Silicon Carbide. *J. Nucl. Mater.* **2011**, *408*, 257−271.

(8) Kohler, C. Atomistic Modelling of Structures of Tilt Grain Boundaries and Antiphase Boundaries in β-Silicon Carbide. *Phys. Status Solidi B* **2002**, *234*, 522−540.
(9) Kohyama, M.; Kose, S.; Yamamoto, R. Theoretical Study of Polar Interfaces of the (122) Σ=9 Grain Boundary in Cubic SiC. *J. Phys.: Condens. Matter* **1991**, *3*, 7555−7573.
(10) Kohyama, M.; Tanaka, K. Ab Initio Study of Grain Boundaries in SiC and Si. *Mater. Sci. Forum* **1999**, *294*−*296*, 231−234.
(11) Shrader, D.; Szlufarska, I.; Morgan, D. Cs Diffusion in Cubic Silicon Carbide. *J. Nucl. Mater.* **2012**, *421*, 89−96.
(12) Khalil, S.; Swaminathan, N.; Shrader, D.; Heim, A. J.; Morgan, D. D.; Szlufarska, I. Diffusion of Ag Along Σ3 Grain Boundaries in 3C-SiC. *Phys. Rev. B* **2011**, *84*, 214104.
(13) Krack, M.; Parrinello, M. Quickstep: Make the Atoms Dance. In *High Performance Computing in Chemistry*, Grotendorst, J., Ed.; NIC-Directors: Jülich, Germany, 2004; Vol. *25*, pp 29−51.
(14) VandeVondele, J.; Krack, M.; Mohamed, F.; Parrinello, M.; Chassaing, T.; Hutter, J. Quickstep: Fast and Accurate Density Functional Calculations Using a Mixed Gaussian and Plane Waves Approach. *Comput. Phys. Commun.* **2005**, *167*, 103−128.
(15) *CP2K Developers Group*, http://www.cp2k.org: 2000−2012.
(16) Lippert, G.; Hutter, J.; Parrinello, M. A Hybrid Gaussian and Plane Wave Density Functional Scheme. *Mol. Phys.* **1997**, *92*, 477−487.
(17) Perdew, J. P.; Burke, K.; Ernzerhof, M. Generalized Gradient Approximation Made Simple. *Phys. Rev. Lett.* **1996**, *77*, 3865−3868.
(18) Goedecker, S.; Teter, M.; Hutter, J. Separable Dual-Space Gaussian Pseudopotentials. *Phys. Rev. B* **1996**, *54*, 1703−1710.
(19) Hartwigsen, C.; Goedecker, S.; Hutter, J. Relativistic Separable Dual-Space Gaussian Pseudopotentials from H to Rn. *Phys. Rev. B* **1998**, *58*, 3641−3662.
(20) Krack, M. Pseudopotentials for H to Kr Optimized for Gradient-Corrected Exchange-Correlation Functionals. *Theor. Chem. Acc.* **2005**, *114*, 145−152.
(21) VandeVondele, J.; Hutter, J. An Efficient Orbital Transformation Method for Electronic Structure Calculations. *J. Chem. Phys.* **2003**, *118*, 4365−4369.
(22) VandeVondele, J.; Hutter, J. Gaussian Basis Sets for Accurate Calculations on Molecular Systems in Gas and Condensed Phases. *J. Chem. Phys.* **2007**, *127*, 114105.
(23) Boys, S. F.; Bernardi, F. The Calculation of Small Molecular Interactions by the Differences of Separate Total Energies. Some Procedures with Reduced Errors. *Mol. Phys.* **1970**, *19*, 553−566.
(24) Kresse, G.; Furthmüller, J. Efficient Iterative Schemes for Ab Initio Total-Energy Calculations Using a Plane-Wave Basis Set. *Phys. Rev. B* **1996**, *54*, 11169−11186.
(25) Kresse, G.; Furthmüller, J. Efficiency of Ab-Initio Total Energy Calculations for Metals and Semiconductors Using a Plane-Wave Basis Set. *Comput. Mater. Sci.* **1996**, *6*, 15−50.
(26) Kresse, G.; Hafner, J. Ab Initio Molecular Dynamics for Liquid Metals. *Phys. Rev. B* **1993**, *47*, 558−561.
(27) Kresse, G.; Hafner, J. Ab Initio Molecular-Dynamics Simulation of the Liquid-Metal-Amorphous-Semiconductor Transition in Germanium. *Phys. Rev. B* **1994**, *49*, 14251−14269.
(28) Kresse, G.; Joubert, D. From Ultrasoft Pseudopotentials to the Projector Augmented-Wave Method. *Phys. Rev. B* **1999**, *59* (3), 1758−1775.
(29) Kolafa, J. Time-Reversible Always Stable Predictor-Corrector Method for Molecular Dynamics of Polarizable Molecules. *J. Comput. Chem.* **2004**, *25*, 335−342.
(30) Bussi, G.; Donadio, D.; Parrinello, M. Canonical Sampling through Velocity Rescaling. *J. Chem. Phys.* **2007**, *126*, 014101.
(31) Kirchhofer, R.; Cawley, J. D.; Demkowicz, P. A.; Cole, J. I.; Gorman, B. P. Microstructure of TRISO Coated Particles from the AGR-1 Experiment: SiC Grain Size and Grain Boundary Character. *J. Nucl. Mater.* **2013**, *432*, 127−134.
(32) Tan, L.; Allen, T. R.; Hunn, J. D.; Miller, J. H. EBSD for Microstructure and Property Characterization of the SiC-Coating in TRISO Fuel Particles. *J. Nucl. Mater.* **2008**, *372*, 400−404.
(33) Iannuzzi, M.; Laio, A.; Parrinello, M. Reactive Car-Parrinello Molecular Dynamics. *Phys. Rev. Lett.* **2003**, *90*, 238302.
(34) Laio, A.; Parrinello, M. Escaping Free-Energy Minima. *Proc. Natl. Acad. Sci. U.S.A.* **2002**, *99*, 12562−12566.
(35) Rintelman, J. M.; Gordon, M. S. Structure and Energetics of the Silicon Carbide Clusters SiC_3 and Si_2C_2. *J. Chem. Phys.* **2001**, *115*, 1795−1803.
(36) Henkelman, G.; Arnaldsson, A.; Jonsson, H. A Fast and Robust Algorithm for Bader Decomposition of Charge Density. *Comput. Mater. Sci.* **2006**, *36*, 254−360.
(37) Sanville, E.; Kenny, S.; Smith, R.; Henkelman, G. An Improved Grid-Based Algorithm for Bader Charge Allocation. *J. Comput. Chem.* **2007**, *28*, 899−908.
(38) Tang, W.; Sanville, E.; Henkelman, G.; Grid-Based Bader, A. Analysis Algorithm without Lattice Bias. *J. Phys.: Condens. Matter* **2009**, *21*, 084204.
(39) Allelein, H.-J. *Spaltproduktverhalten - Speziell Cs-137 in HTR TRISO Brennstoffteilchen*. Berichte der Kernforschungsanlage Jülich: Jülich, Germany, 1980; p 148.
(40) Amian, W.; Stover, D. Diffusion of Silver and Cesium in Silicon-Carbide Coatings of Fuel Particles for High-Temperature Gas-Cooled Reactors. *Nucl. Technol.* **1983**, *61*, 475−486.
(41) IAEA. *Fuel Performance and Fission Produce Behaviour in Gas Cooled Reactors*. Vienna, Austria, 1997. IAEA-TECDOC-978.
(42) Londono-Hurtado, A.; Heim, A. J.; Kim, S.; Szlufarska, I.; Morgan, D. Cs and Ag Co-Incorporation in Cubic Silicon Carbide. *J. Nucl. Mater.* **2013**, *439*, 65−71.